ACS APPLIED MATERIALS & INTERFACES

Research Article

www.acsami.org

Do Transition Metal Carbonates Have Greater Lithium Storage Capability Than Oxides? A Case Study of Monodisperse $CoCO_3$ and CoO Microspindles

Lianbang Wang,[†] Weijie Tang,[†] Yu Jing,[‡] Liwei Su,*[,†] and Zhen Zhou*[,‡]

[†]State Key Laboratory Breeding Base of Green Chemistry-Synthesis Technology, College of Chemical Engineering, Zhejiang University of Technology, Hangzhou 310014, China

[‡]Tianjin Key Laboratory of Metal and Molecule Based Material Chemistry, Key Laboratory of Advanced Energy Materials Chemistry (Ministry of Education), Institute of New Energy Material Chemistry, Collaborative Innovation Center of Chemical Science and Engineering (Tianjin), Nankai University, Tianjin 300071, China

Supporting Information

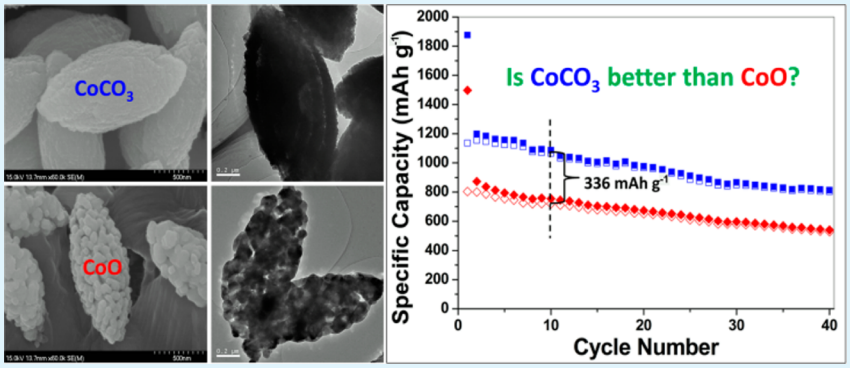

ABSTRACT: As substitutions for transition metal oxides (MOs), transition metal carbonates (MCO_3) have been attracting more and more attention because of their lithium storage ability in recent years. Is MCO_3 better than MOs for lithium storage? To answer this question, monodisperse $CoCO_3$ and CoO microspindles with comparable structures were synthesized and investigated as a case study. Excluding its structural effect, we found $CoCO_3$ still exhibited reversible capacities and rate capabilities much higher than those of CoO. The reversible capacity of $CoCO_3$ after 10 cycles was 1065 mAh g^{-1}, 48.2% higher than that (~720 mAh g^{-1}) of CoO. Furthermore, the greatly different electrochemical behaviors were investigated by analyzing the discharge−charge profiles, cyclic voltammetry curves, and Nyquist plots in depth. This work can improve our understanding of the lithium storage advantages of MCO_3 against MOs and enlighten us in terms of developing high-performance MCO_3 with favorable structures.

KEYWORDS: *anodes, batteries, lithium storage, transition metal carbonates, transition metal oxides*

INTRODUCTION

Lithium ion batteries (LIBs) are currently powerful and promising devices for increasing the diversity of portable electric applications because of the high energy and power density, good safety, and environmental benignity.[1−4] Tremendous effort has been spent in developing advanced anode materials to substitute for the commercial graphite anode with a low theoretical capacity (372 mAh g^{-1} for LiC_6) and unsatisfactory rate performance.[5−7] In 2000, Tarascon's group introduced transition metal oxides (MOs) as LIB anodes and proposed a conversion mechanism in which MOs can reversibly decompose to M^0/Li_2O and contribute specific capacities (generally 700−1100 mAh g^{-1}) much higher than that of graphite.[8] Henceforth, almost all the potential MOs (M = Co, Fe, Ni, Cu, Mn, Cr, etc.) were investigated in depth and can approach or even exceed their theoretical capacity with the help of nanotechnology and composite modification.[9−16]

If transition metal carbonates (MCO_3) are adopted as LIB anodes, according to the conversion mechanism, MCO_3 should convert to M^0/Li_2CO_3 when discharging and contribute a limited capacity of ~450 mAh g^{-1}. However, more and more results indicate that MCO_3 has much higher potentials for lithium storage.[17−20] In our previous work, $CoCO_3$/graphene exhibited a high reversible capacity of ~930 mAh g^{-1} (after 40 cycles), more than twice the theoretical value based on the conversion mechanism.[21] In multiple analyses of the electrochemical behaviors by combining experimental measurements

Received: April 8, 2014
Accepted: July 10, 2014
Published: July 10, 2014

and computational simulations, we proposed that Li_2CO_3 can also participate in lithium storage with the catalytic effect of the newly decomposed metal nanoparticles from MCO_3 at appropriate potentials. On the basis of the novel mechanism, MCO_3 can in principle deliver a more promising capacity of ~1300 mAh g^{-1} and hence has attracted more and more attention in recent years.[22−27] For example, rambutan-like $FeCO_3$ hollow microspheres and $FeCO_3$ microrhombohedra exhibited long-term and reversible capacities of ~880 mAh g^{-1} after 100 cycles and 1018 mAh g^{-1} after 120 cycles, respectively.[22,24] Furthermore, with the help of high-conductivity materials, $CoCO_3$/polypyrrole composites demonstrated a reversible capacity of 1070 mAh g^{-1} for 100 cycles, good rate performances, and a recovery capacity of up to 1787 mAh g^{-1} after 500 cycles at 1−5 C.[26] In comparison, the theoretical values of FeO and CoO were only 746 and 718 mAh g^{-1}, respectively. Thus, is MCO_3 better than MOs for lithium storage?

To address this question, we investigated the electrochemical lithium storage behaviors of $CoCO_3$ and CoO as a case study. To avoid the negative effect of morphology and particle size, $CoCO_3$ and CoO were designed with comparable structures. Monodisperse $CoCO_3$ and CoO microspindles (~1.4 μm in length and 0.5−0.7 μm in diameter) were synthesized through a solvothermal route and subsequent sintering. Profiting from the favorable features, both hierarchical $CoCO_3$ and CoO microspindles presented high reversible capacity and considerable cycling stability. Furthermore, the electrochemical behaviors were studied in depth by comparing the discharge−charge curves and the results of cyclic voltammetry (CV), and electrochemical impedance spectroscopy (EIS). This work can improve our understanding of the lithium storage advantages of MCO_3 versus MOs.

EXPERIMENTAL SECTION

Material Synthesis. Monodisperse $CoCO_3$ and CoO microspindles were fabricated through a facile solvothermal treatment and subsequent sintering. All the reagents are analytical grade and used without further purification. In a typical synthesis, 0.299 g of cobaltous acetate, 1.500 g of urea, and 1.405 g of sodium dodecyl benzenesulfonate (SDBS) were homogeneously dispersed in 60 mL of ethylene glycol (EG) under vigorous and ultrasonic agitation for 60 min separately. The suspension was placed to a 100 mL Teflon-sealed autoclave and maintained at 180 °C in an oven for 24 h. The products were centrifuged and washed with ethanol and water at least three times separately and dried at 60 °C. The pink samples were further changed to $CoCO_3$ microspindles at 300 °C for 4 h in an Ar flow. To obtain pure CoO microspindles with comparable structures, $CoCO_3$ precursors were decomposed at a relatively low temperature (400 °C for 4 h) under vacuum.

Material Characterization. The samples were characterized by X-ray diffraction (XRD) [Rigaku D/Max III diffractometer with Cu Kα radiation (λ = 1.5418 Å)], scanning electron microscopy (SEM) (Hitachi S-4700 operated at 15 kV and an FEI Nanosem 430 field-emission gun scanning electron microscope), and thermogravimetric analysis (TG-DTA) (Rigaku PTC-10A TG-DTA analyzer). Transmission electron microscopy (TEM), high-resolution transmission electron microscopy (HRTEM), and selected area electronic diffraction (SAED) were conducted with Tecnai G^2F-30 S-Twin (operated at 300 kV) and FEI Tecnai G^2F-20 field-emission gun transmission electron microscopes.

Electrochemical Measurements. In the test cells, lithium metal was used as the counter and reference electrode. The working electrodes were comprised of active materials, acetylene black (AB), and polytetrafluoroethylene (PTFE) at a weight ratio of 15:3:2. The average weight of the working electrodes is approximately 2 mg. The electrolyte was 1 M $LiPF_6$ dissolved in a 1:1:1 ethylene carbonate (EC)/ethylene methyl carbonate (EMC)/dimethyl carbonate (DMC) mixture. The cells were assembled in a glovebox filled with high-purity argon (O_2 and H_2O at <1 ppm). Discharge−charge measurements of the cells were performed in the potential range of 0.01−3.00 V (vs Li/Li^+) under a LAND-CT2001A instrument at room temperature. CV was performed at a scanning rate of 0.1 mV s^{-1} between 0.01 and 3.00 V (vs Li/Li^+). EIS was conducted with a Solartron SI1287+SI1260 potentiometer at 25 °C with the frequency ranging from 10 kHz to 10 mHz and an AC signal with an amplitude of 5 mV as the perturbation.

RESULTS AND DISCUSSION

Monodisperse $CoCO_3$ and CoO microspindles were fabricated through a facile solvothermal route and subsequent sintering. First, monodisperse $CoCO_3$ was synthesized via a solvothermal procedure by optimizing the temperatures and Co^{2+} concentrations (Figures S1−S3 of the Supporting Information). Then, the prepared microspindles were further sintered at 300 °C in an Ar flow to remove the residue H_2O and improve the crystallinity. As shown via TGA (Figures S4 and S5 of the Supporting Information), the small weight loss before 300 °C corresponds to the removal of the residue H_2O, while the steep slope at ~350 °C indicates the decomposition of $CoCO_3$. As previously reported, pure CoO can be obtained by decomposing $CoCO_3$ at high temperatures (>700 °C) in Ar.[28,29] However, the microspindles were found to be damaged to a great extent, which yield make some negative effects on the comparison of electrochemical behaviors between $CoCO_3$ and CoO. Instead, a low-temperature heating (400 °C) in vacuum was adopted here to decompose $CoCO_3$ to CoO microspindles with comparable structures and sizes.[30,31] The preparation can be schematically illustrated in Scheme 1.

Scheme 1. Illustration of the Preparation of Multilayer $CoCO_3$ and Porous CoO Microspindles

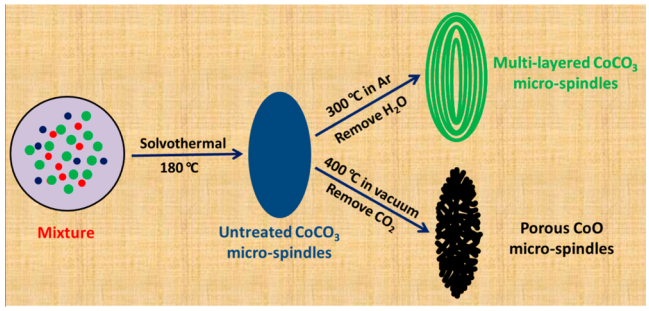

Figure 1 presents the XRD patterns of solvothermal products after two different heating treatments. All the peaks are well assigned to the standard cards of pure $CoCO_3$ and CoO, indicating no impurity existed. The main peaks of the product (300 °C) at 25.0°, 32.6°, and 53.8° belong to (0 1 2), (1 0 4), and (1 1 6) planes, respectively, of rhombohedral $CoCO_3$ (JCPDS Card No. 11-0692), while the peaks of the product (400 °C) at 36.5°, 42.4°, 61.5°, and 73.7° correspond to (1 1 1), (2 0 0), (2 2 0), and (3 1 1) planes, respectively, of cubic CoO (JCPDS Card No. 43-1004).

Figure 2 shows the morphology and inner structure of $CoCO_3$ products. It is clear that $CoCO_3$ microspindles possess a good distribution (~1.4 μm in length and ~0.7 μm in diameter) without obvious agglomeration (Figure 2A,B). Furthermore, these microspindles have a rough surface consisting of thousands of $CoCO_3$ nanoparticles (Figure 2C).

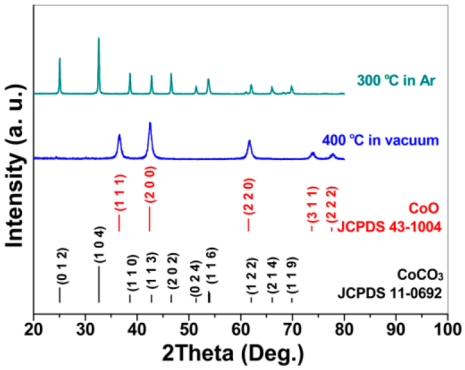

Figure 1. XRD patterns of the solvothermal products after being heated at 300 °C in Ar ($CoCO_3$) and 400 °C under vacuum (CoO).

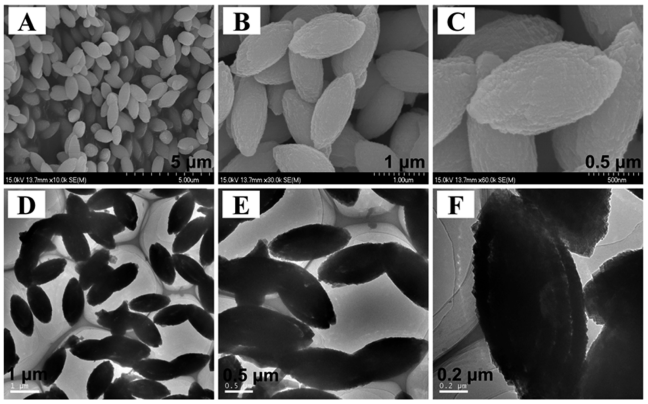

Figure 2. SEM (A–C) and TEM (D–F) images of $CoCO_3$ microspindles.

In fact, TEM images demonstrate that all the $CoCO_3$ microspindles are not solid single crystalline but composed of some layers full of $CoCO_3$ nanoparticles (Figure 2D–F). To further confirm this conclusion, $CoCO_3$ microspindles were manually gridded for 2 min and totally changed to very small nanoparticles (generally 10–30 nm) (Figure 3A,B), in agreement with the SEM and TEM results mentioned above. Note that some research groups have also noticed the hierarchical multilayer or hollow MCO_3 microparticles in recent years and ascribed their formation to the gas templates and Ostwald ripening process in the solution as well as the Kirkendall effect during sintering.[22,32−37] In this work, the three factors might function at the same time. (1) Urea in the mixture solution decomposed into CO_2 and NH_3 first. On one hand, CO_2 can react with Co^{2+} to form $CoCO_3$ nanocystals; on the other, more CO_2 might absorb on the surface of $CoCO_3$ and serve as the gas templates for the formation of another $CoCO_3$ layer. (2) Ostwald ripening plays an essential role in the solvothermal treatment, during which small $CoCO_3$ nanocyrstals trend to grow into larger particles and hence enlarge the space between layers. (3) Both the release of H_2O residue and the increase in the crystallinity during sintering increase the density of $CoCO_3$ and hence benefit the formation of the multilayer structure.

The prepared $CoCO_3$ and CoO microspindles were assembled into working electrodes and tested at 0.01–3.0 V (Figure 3C,D). When the microspindles were cycled at 50 mA g^{-1}, the initial discharge–charge capacities were 1875.9 and 1135.4 mAh g^{-1} with a Coulombic efficiency of 60.5% (Figure 3C). The reversible capacity was maintained over 800 mAh g^{-1} during the initial 40 cycles, indicating the Li–$CoCO_3$ reaction exhibits good reversibility and high capability for energy storage. Even at 200 and 500 mA g^{-1}, the reversible capacities after 40 cycles still remained at 638 and 469 mAh g^{-1},

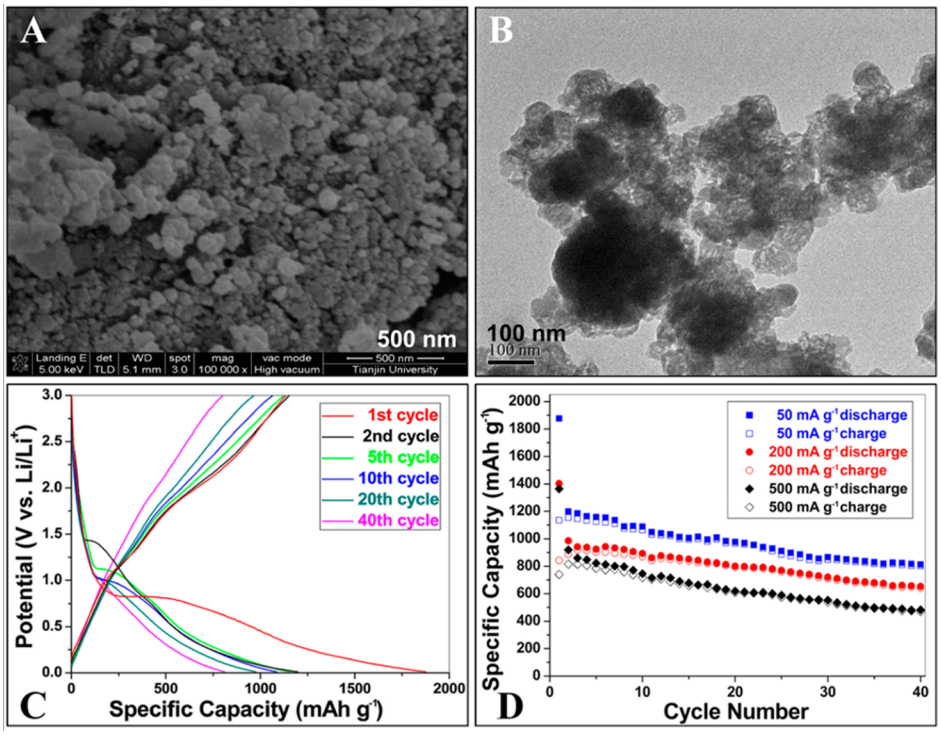

Figure 3. SEM (A) and TEM (B) images of $CoCO_3$ microspindles after being ground for 2 min. (C) Charge–discharge profiles at 50 mA g^{-1} and (D) cycling performance at different current densities of $CoCO_3$ microspindles.

respectively (Figure 3D). The considerable performances can be attributed to the favorable hierarchical structure of $CoCO_3$ microspindles. (1) Large microspindles consisting of thousands of $CoCO_3$ nanocrystals (10−30 nm) provide a better electron/Li^+ transport and a reduced absolute volume variation in comparison with bulk ones. (2) The multilayer structures can further accommodate the volume swings during the repeated lithiation−delithiation processes and hence maintain the support integrity to a great extent. Similar hollow or multilayer structures have been widely adopted for the preparation of high-performance LIB anodes, especially MOs and SnO_2.[38−42]

Does $CoCO_3$ have better lithium storage capability than CoO? To obtain comparable CoO structures, $CoCO_3$ microspindles were slowly decomposed at a relatively low temperature (400 °C) under vacuum. Along with the gradual release of CO_2, the close-grained $CoCO_3$ surface changed to a porous structure, while the diameter of microspindles decreased to ∼0.5 μm (Figure 4A,B). TEM images further reveal that

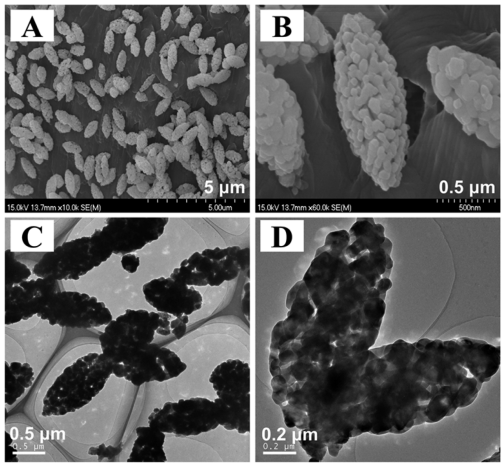

Figure 4. SEM (A and B) and TEM (C and D) images of CoO microspindles.

multilayer microspindles were totally transformed into porous microspindles, while $CoCO_3$ nanocrystals (10−30 nm) grew into larger CoO nanoparticles (40−100 nm) (Figure 4C,D). HRTEM and SAED demonstrated both $CoCO_3$ and CoO are quite crystalline (Figure S6 of the Supporting Information). No obvious impurities were observed. The variation in morphology can be attributed to the release of CO_2 from $CoCO_3$ and the increasing crystallinity of CoO.[28,43,44] In summary, $CoCO_3$ and CoO microspindles possess a comparable structure for comparison of their electrochemical behaviors.

Profiting from similar hierarchical structures, porous CoO microspindles also presented a high reversible capacity and considerable stability. At 50 mA g^{-1}, the initial discharge−charge capacities were 1497.5 and 803.8 mAh g^{-1} with a Coulombic efficiency (53.7%) lower than that of $CoCO_3$ (Figure 5A). The reversible capacity remained at 528 mAh g^{-1} after 40 cycles. Note that the capacities of both $CoCO_3$ and CoO gradually decreased along with repeated cycling, because of the unsatisfactory electronic conductivity and the lack of passivation layers for the huge volume variation. Notable among these is the fact that the reversible capacity of $CoCO_3$ after 10 cycles is 1065 mAh g^{-1}, 48.2% higher than the value (∼720 mAh g^{-1}) of CoO. Also, $CoCO_3$ exhibited better Coulombic efficiency and rate capability. Thus, why does $CoCO_3$ have better lithium storage capability than CoO? The discharge−charge behaviors were investigated in depth by comparing the discharge−charge profiles, CV curves, and EIS spectra (Figure 5B−D). The initial discharge profile and cathodic CV curve of $CoCO_3$ and CoO greatly differ from the subsequent ones, referring to the irreversible formation of the solid−electrolyte interface (SEI) film that mainly grows during the first discharge process below 1.0 V (Figure 5B,C).[45−47] Although $CoCO_3$ and CoO have similar SEI formation and irreversible capacities of ∼700 mAh g^{-1} in the first discharge, they presented totally different discharge−charge and CV curves as well as corresponding redox reactions during the following cycles. Contrary to the direct conversion from CoO to Co^0/Li_2O, the lithiation of $CoCO_3$ can be divided into two parts. (1) $CoCO_3$ decomposes to Co^0 and Li_2CO_3. (2) C^{4+} in Li_2CO_3 is further reduced to other low-valence C elements under the catalytic effect of the newly generated Co^0 nanoparticles at appropriate potentials; this process has been preliminarily confirmed in many reports (Figure S7 of the Supporting Information).[21,24−26] Accordingly, the discharge−charge and CV curves exhibit two couples of potential platforms and/or peaks at 1.8−2.2 and 1.0−1.4 V. The obvious potential differences at discharge and charge processes can be attributed to the great polarization along with electron storage, which tremendously existed in anode materials, especially transition metal compounds.[47−49] Note that similar catalytic reactions also exist beyond C^{4+} in Li_2CO_3. For example, Rangasamy et al. reported that the Li_3PS_4 solid electrolyte could contribute an additional capacity by reducing the valence of P^{5+} to P^{4+} in the presence of the LiF catalyst.[50] Hu et al. also reported that LiOH, one of the SEI components, can react with Li to form Li_2O and LiH in the presence of Ru^0.[51]

Note that EIS spectra imply that $CoCO_3$ electrodes have electron transport and Li^+ ion diffusion similar to or poorer than that of CoO, especially after cycling (Figure 5D, Figure S8 and Table S1 of the Supporting Information). Moreover, considering the insertion of more Li^+, $CoCO_3$ should have an expansion of volume larger than that of CoO, although no direct data were reported, to the best of our knowledge. Thus, why did $CoCO_3$ present much higher capacities than CoO? In fact, the higher lithium storage capability of $CoCO_3$ did not come from a better electron−Li^+ transfer but was ascribed to its theoretical value being much higher than that of CoO. According to the aforementioned electrochemical catalytic conversion mechanism, $CoCO_3$ theoretically has lithium storage potentials (1350 mAh g^{-1} for Co^{2+} to Co^0 and C^{4+} to C^0) much higher than that of CoO (718 mAh g^{-1} for Co^{2+} to Co^0). Therefore, the poorer electron−Li^+ transfer did not conflict with the conclusion that the electrochemical performance of $CoCO_3$ is better than that of CoO. By contrast, the difficulties in the kinetics and volume variation make it clear that $CoCO_3$ has many more lithium storage sites than CoO, which can satisfactorily explain all the electrochemical behaviors of $CoCO_3$ and CoO in this work. Also, we prepared MCO_3 and the counterpart MOs ($MnCO_3$−MnO and $FeCO_3$−Fe_2O_3) and compared their electrochemical performances (Figure S9 of the Supporting Information). Taken together, we believe that MCO_3 has higher lithium storage capability than MOs. An effective strategy for minimizing the electron−Li^+ transfer resistance and volume expansion is preparing $CoCO_3$ nanoparticles and combining them with high-conductivity materials such as conductive polymers, pyrolysis carbon, carbon nanotubes, and graphene.[1,52−54]

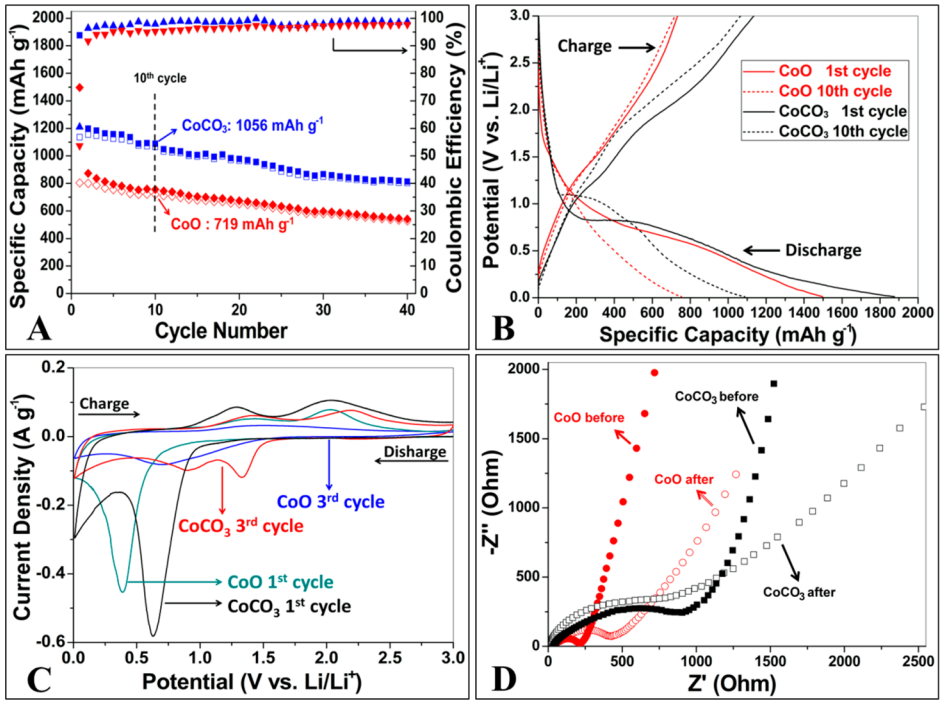

Figure 5. Comparison on the electrochemical lithium storage behaviors of $CoCO_3$ and CoO microspindles: cycling performances at 50 mA g^{-1} (A), charge−discharge profiles at 50 mA g^{-1} (B), CV curves (C), and Nyquist plots before cycling and after three cycles (D).

CONCLUSION

In summary, to compare the electrochemical lithium storage behaviors of MCO_3 and MOs, monodisperse $CoCO_3$ and CoO microspindles with comparable structures were synthesized through a facile solvothermal treatment and subsequent sintering. Profiting from the hierarchical multilayer and porous features, both $CoCO_3$ and CoO exhibited a high reversible capacity and considerable stability. Note that the reversible capacity of $CoCO_3$ after 10 cycles is 1065 mAh g^{-1}, 48.2% higher than that (~720 mAh g^{-1}) of CoO. Furthermore, $CoCO_3$ and CoO demonstrated greatly different electrochemical behaviors, including the discharge−charge profiles, CV curves, and EIS spectra, indicating that $CoCO_3$ has much greater capability for lithium storage than CoO. Also, $CoCO_3$ possesses similar electron−Li^+ transfer and larger volume variation during the discharge−charge process than CoO, which restricts its capacity and cycling stability to a great extent. Preparing $CoCO_3$ nanoparticles and combining them with high-conductivity materials can effectively overcome these shortcomings. This work can improve our understanding of the lithium storage advantages of MCO_3 against MOs and enlighten us in terms of developing high-performance MCO_3 with favorable structures.

ASSOCIATED CONTENT

Supporting Information

XRD patterns, SEM images of the solvothermal products under different conditions, TGA curves of $CoCO_3$, HRTEM and SAED of $CoCO_3$ and CoO, Nyquist plots and equivalent circuit, and electrochemical performances of $MnCO_3$-MnO and $FeCO_3$-Fe_2O_3. This material is available free of charge via the Internet at http://pubs.acs.org.

AUTHOR INFORMATION

Corresponding Authors

*E-mail: suliwei@zjut.edu.cn.
*E-mail: zhouzhen@nankai.edu.cn.

Notes

The authors declare no competing financial interest.

ACKNOWLEDGMENTS

This work was supported by the Research Fund for the Doctoral Program of Higher Education of China (20120031110008), the MOE Innovation Research Team (IRT-13R30), and the International Science and Technology Cooperation Program of China (2012C14027).

REFERENCES

(1) Su, L.; Jing, Y.; Zhou, Z. Li Ion Battery Materials with Core-Shell Nanostructures. *Nanoscale* **2011**, *3*, 3967−3983.
(2) Scrosati, B.; Hassoun, J.; Sun, Y. K. Lithium-Ion Batteries. A Look into the Future. *Energy Environ. Sci.* **2011**, *4*, 3287−3295.
(3) Tarascon, J.-M.; Armand, M. Issues and Challenges Facing Rechargeable Lithium Batteries. *Nature* **2001**, *414*, 359−367.
(4) Hong, S. Y.; Kim, Y.; Park, Y.; Choi, A.; Choi, N.-S.; Lee, K. T. Charge Carriers in Rechargeable Batteries: Na Ions vs. Li Ions. *Energy Environ. Sci.* **2013**, *6*, 2067−2081.
(5) Ji, L.; Lin, Z.; Alcoutlabi, M.; Zhang, X. Recent Developments in Nanostructured Anode Materials for Rechargeable Lithium-Ion Batteries. *Energy Environ. Sci.* **2011**, *4*, 2682−2699.
(6) Zhang, P.; Wang, L.; Xie, J.; Su, L.; Ma, C. a. Micro/Nano-Complex-Structure SiO_x-PANI-Ag Composites with Homogeneously-Embedded Si Nanocrystals and Nanopores as High-Performance Anodes for Lithium Ion Batteries. *J. Mater. Chem. A* **2014**, *2*, 3776−3782.
(7) Su, L. W.; Zhou, Z.; Ren, M. M. Core Double-Shell Si@SiO_2@C Nanocomposites as Anode Materials for Li-Ion Batteries. *Chem. Commun.* **2010**, *46*, 2590−2592.

(8) Poizot, P.; Laruelle, S.; Grugeon, S.; Dupont, L.; Tarascon, J. M. Nano-Sized Transition-Metal Oxides as Negative-Electrode Materials for Lithium-Ion Batteries. *Nature* **2000**, *407*, 496−499.
(9) Su, L.; Zhong, Y.; Zhou, Z. Role of Transition Metal Nanoparticles in Extra Lithium Storage Capacity of Transition Metal Oxides: A Case Study of Hierarchical Core-Shell Fe_3O_4@C and Fe@C Microspheres. *J. Mater. Chem. A* **2013**, *1*, 15158−15166.
(10) Yuan, S. M.; Li, J. X.; Yang, L. T.; Su, L. W.; Liu, L.; Zhou, Z. Preparation and Lithium Storage Performances of Mesoporous Fe_3O_4@C Microcapsules. *ACS Appl. Mater. Interfaces* **2011**, *3*, 705−709.
(11) Su, L.; Zhong, Y.; Wei, J.; Zhou, Z. Preparation and Electrochemical Li Storage Performance of MnO@C Nanorods Consisting of Ultra Small MnO Nanosrystals. *RSC Adv.* **2013**, *3*, 9035−9041.
(12) Ren, M.; Yuan, S.; Su, L.; Zhou, Z. Chrysanthemum-Like Co_3O_4 Architectures: Hydrothermal Synthesis and Lithium Storage Performances. *Solid State Sci.* **2012**, *14*, 451−455.
(13) Jiang, L.-Y.; Xin, S.; Wu, X.-L.; Li, H.; Guo, Y.-G.; Wan, L.-J. Non-Sacrificial Template Synthesis of Cr_2O_3−C Hierarchical Core/Shell Nanospheres and Their Application as Anode Materials in Lithium-Ion Batteries. *J. Mater. Chem.* **2010**, *20*, 7565−7569.
(14) Yin, Z.; Ding, Y.; Zheng, Q.; Guan, L. CuO/Polypyrrole Core-Shell Nanocomposites as Anode Materials for Lithium-Ion Batteries. *Electrochem. Commun.* **2012**, *20*, 40−43.
(15) Liu, L.; Li, Y.; Yuan, S. M.; Ge, M.; Ren, M. M.; Sun, C. S.; Zhou, Z. Nanosheet-Based NiO Microspheres: Controlled Solvothermal Synthesis and Lithium Storage Performances. *J. Phys. Chem. C* **2010**, *114*, 251−255.
(16) Sun, X.; Yan, C.; Chen, Y.; Si, W.; Deng, J.; Oswald, S.; Liu, L.; Schmidt, O. G. Three-Dimensionally "Curved" NiO Nanomembranes as Ultrahigh Rate Capability Anodes for Li-Ion Batteries with Long Cycle Lifetimes. *Adv. Energy Mater.* **2014**, *4*, DOI: 10.1002/aenm.201300912.
(17) Aragón, M. J.; León, B.; Pérez Vicente, C.; Tirado, J. L. A New Form of Manganese Carbonate for the Negative Electrode of Lithium-Ion Batteries. *J. Power Sources* **2011**, *196*, 2863−2866.
(18) Aragón, M. J.; Pérez-Vicente, C.; Tirado, J. L. Submicronic Particles of Manganese Carbonate Prepared in Reverse Micelles: A New Electrode Material for Lithium-Ion Batteries. *Electrochem. Commun.* **2007**, *9*, 1744−1748.
(19) Mirhashemihaghighi, S.; Leon, B.; Perez Vicente, C.; Tirado, J. L.; Stoyanova, R.; Yoncheva, M.; Zhecheva, E.; Saez Puche, R.; Arroyo, E. M.; Romero de Paz, J. Lithium Storage Mechanisms and Effect of Partial Cobalt Substitution in Manganese Carbonate Electrodes. *Inorg. Chem.* **2012**, *51*, 5554−5560.
(20) Sharma, Y.; Sharma, N.; Rao, G. V. S.; Chowdari, B. V. R. Nano-$(Cd_{1/3}Co_{1/3}Zn_{1/3})CO_3$: A New and High Capacity Anode Material for Li-Ion Batteries. *J. Mater. Chem.* **2009**, *19*, 5047−5054.
(21) Su, L.; Zhou, Z.; Qin, X.; Tang, Q.; Wu, D.; Shen, P. $CoCO_3$ Submicrocube/Graphene Composites with High Lithium Storage Capability. *Nano Energy* **2013**, *2*, 276−282.
(22) Zhong, Y.; Su, L.; Yang, M.; Wei, J.; Zhou, Z. Rambutan-like $FeCO_3$ Hollow Microspheres: Facile Preparation and Superior Lithium Storage Performances. *ACS Appl. Mater. Interfaces* **2013**, *5*, 11212−11217.
(23) Shao, L.; Wu, K.; Jiang, X.; Shui, M.; Ma, R.; Lao, M.; Lin, X.; Wang, D.; Long, N.; Shu, J. Preparation and Characterization of Basic Carbonates as Novel Anode Materials for Lithium-Ion Batteries. *Ceram. Int.* **2014**, *40*, 3105−3116.
(24) Zhao, S.; Yu, Y.; Wei, S.; Wang, Y.; Zhao, C.; Liu, R.; Shen, Q. Hydrothermal Synthesis and Potential Applicability of Rhombohedral Siderite as a High-Capacity Anode Material for Lithium Ion Batteries. *J. Power Sources* **2014**, *253*, 251−255.
(25) Shao, L.; Ma, R.; Wu, K.; Shui, M.; Lao, M.; Wang, D.; Long, N.; Ren, Y.; Shu, J. Metal Carbonates as Anode Materials for Lithium Ion Batteries. *J. Alloys Compd.* **2013**, *581*, 602−609.
(26) Ding, Z.; Yao, B.; Feng, J.; Zhang, J. Enhanced Rate Performance and Cycling Stability of a $CoCO_3$−Polypyrrole Composite for Lithium Ion Battery Anodes. *J. Mater. Chem. A* **2013**, *1*, 11200−11209.
(27) Zhang, F.; Zhang, R.; Feng, J.; Qian, Y. $CdCO_3$/Carbon Nanotube Nanocomposites as Anode Materials for Advanced Lithium-Ion Batteries. *Mater. Lett.* **2014**, *114*, 115−118.
(28) Jamil, S.; Jing, X.; Wang, J.; Li, S.; Liu, J.; Zhang, M. The Synthesis of Porous Co_3O_4 Micro Cuboid Structures by Solvothermal Approach and Investigation of Its Gas Sensing Properties and Catalytic Activity. *Mater. Res. Bull.* **2013**, *48*, 4513−4520.
(29) Wang, G. X.; Chen, Y.; Konstantinov, K.; Lindsay, M.; Liu, H. K.; Dou, S. X. Investigation of Cobalt Oxides as Anode Materials for Li-Ion Batteries. *J. Power Sources* **2002**, *109*, 142−147.
(30) Wu, J.; Tu, J.; Wang, X.; Zhang, W. Synthesis of Nanoscale CoO Particles and Their Effect on the Positive Electrodes of Nickel−Metal Hydride Batteries. *Int. J. Hydrogen Energy* **2007**, *32*, 606−610.
(31) Wu, J. B.; Tu, J. P.; Han, T. A.; Yang, Y. Z.; Zhang, W. K.; Zhao, X. B. High-Rate Dischargeability Enhancement of Ni/MH Rechargeable Batteries by Addition of Nanoscale CoO to Positive Electrodes. *J. Power Sources* **2006**, *156*, 667−672.
(32) Cai, R.; Du, Y.; Peng, S.; Bi, H.; Zhang, W.; Yang, D.; Chen, J.; Lim, T. M.; Zhang, H.; Cao, Y. C.; Yan, Q. Synthesis of Porous, Hollow Metal MCO_3 (M = Mn, Co, Ca) Microstructures and Adsorption Properties Thereof. *Chem.—Eur. J.* **2014**, *20*, 421−425.
(33) Liu, L.; Yang, Z.; Liang, H.; Yang, H.; Yang, Y. Facile Synthesis of $MnCO_3$ Hollow Dumbbells and Their Conversion to Manganese Oxide. *Mater. Lett.* **2010**, *64*, 2060−2063.
(34) Cao, J.; Mao, Q.; Shi, L.; Qian, Y. Fabrication of γ-MnO_2/α-MnO_2 Hollow Core/Shell Structures and Their Application to Water Treatment. *J. Mater. Chem.* **2011**, *21*, 16210−16215.
(35) Fei, J. B.; Cui, Y.; Yan, X. H.; Qi, W.; Yang, Y.; Wang, K. W.; He, Q.; Li, J. B. Controlled Preparation of MnO_2 Hierarchical Hollow Nanostructures and Their Application in Water Treatment. *Adv. Mater.* **2008**, *20*, 452−456.
(36) Xu, M.-W.; Niu, Y.-B.; Bao, S.-J.; Li, C. M. An Architectural Development for Energy Conversion Materials: Morphology-Conserved Transformation Synthesis of Manganese Oxides and Their Application in Lithium Ion Batteries. *J. Mater. Chem. A* **2014**, *2*, 3749−3746.
(37) Wang, L.; Tang, F.; Ozawa, K.; Chen, Z. G.; Mukherj, A.; Zhu, Y.; Zou, J.; Cheng, H. M.; Lu, G. Q. A General Single-Source Route for the Preparation of Hollow Nanoporous Metal Oxide Structures. *Angew. Chem., Int. Ed.* **2009**, *48*, 7048−7051.
(38) Lai, X.; Halpert, J. E.; Wang, D. Recent Advances in Micro-/Nano-Structured Hollow Spheres for Energy Applications: From Simple to Complex Systems. *Energy Environ. Sci.* **2012**, *5*, 5604−5018.
(39) Lou, X. W.; Li, C. M.; Archer, L. A. Designed Synthesis of Coaxial SnO_2@Carbon Hollow Nanospheres for Highly Reversible Lithium Storage. *Adv. Mater.* **2009**, *21*, 2536−2539.
(40) Park, M.-H.; Kim, K.; Kim, J.; Cho, J. Flexible Dimensional Control of High-Capacity Li-Ion-Battery Anodes: From 0D Hollow to 3D Porous Germanium Nanoparticle Assemblies. *Adv. Mater.* **2010**, *22*, 415−418.
(41) Wang, B.; Chen, J. S.; Wu, H. B.; Wang, Z.; Lou, X. W. Quasiemulsion-Templated Formation of α-Fe_2O_3 Hollow Spheres with Enhanced Lithium Storage Properties. *J. Am. Chem. Soc.* **2011**, *133*, 17146−17148.
(42) Ding, S.; Zhang, D.; Wu, H. B.; Zhang, Z.; Lou, X. W. Synthesis of Micro-Sized SnO_2@Carbon Hollow Spheres with Enhanced Lithium Storage Properties. *Nanoscale* **2012**, *4*, 3651−3654.
(43) Kokubu, T.; Oaki, Y.; Hosono, E.; Zhou, H.; Imai, H. Biomimetic Solid-Solution Precursors of Metal Carbonate for Nanostructured Metal Oxides: MnO/Co and MnO-CoO Nanostructures and Their Electrochemical Properties. *Adv. Funct. Mater.* **2011**, *21*, 3673−3680.
(44) Xuan, S. H.; Hao, L. Y.; Jiang, W. Q.; Song, L.; Hu, Y.; Chen, Z. Y.; Fei, L. F.; Li, T. W. A $FeCO_3$ Precursor-Based Route to Microsized Peanutlike Fe_3O_4. *Cryst. Growth Des.* **2007**, *7*, 430−434.
(45) Su, L.; Zhou, Z.; Shen, P. Ni/C Hierarchical Nanostructures with Ni Nanoparticles Highly Dispersed in N-Containing Carbon

Nanosheets: Origin of Li Storage Capacity. *J. Phys. Chem. C* **2012**, *116*, 23974−23980.
(46) Su, L.; Zhou, Z.; Shen, P. Core−Shell Fe@Fe_3C/C Nanocomposites as Anode Materials for Li Ion Batteries. *Electrochim. Acta* **2013**, *87*, 180−185.
(47) Laruelle, S.; Grugeon, S.; Poizot, P.; Dollé, M.; Dupont, L.; Tarascon, J. M. On the Origin of the Extra Electrochemical Capacity Displayed by MO/Li Cells at Low Potential. *J. Electrochem. Soc.* **2002**, *149*, A627−A634.
(48) Reddy, M. V.; Yu, T.; Sow, C. H.; Shen, Z. X.; Lim, C. T.; Subba Rao, G. V.; Chowdari, B. V. R. α-Fe_2O_3 Nanoflakes as an Anode Material for Li-Ion Batteries. *Adv. Funct. Mater.* **2007**, *17*, 2792−2799.
(49) Zhen, M.; Su, L.; Yuan, Z.; Liu, L.; Zhou, Z. Well-Distributed TiO_2 Nanocrystals on Reduced Graphene Oxides as High-Performance Anode Materials for Lithium Ion Batteries. *RSC Adv.* **2013**, *3*, 13696−13701.
(50) Rangasamy, E.; Li, J.; Sahu, G.; Dudney, N.; Liang, C. Pushing the Theoretical Limit of Li-CF x Batteries: A Tale of Bifunctional Electrolyte. *J. Am. Chem. Soc.* **2014**, *136*, 6874−6877.
(51) Hu, Y. Y.; Liu, Z.; Nam, K. W.; Borkiewicz, O. J.; Cheng, J.; Hua, X.; Dunstan, M. T.; Yu, X.; Wiaderek, K. M.; Du, L. S.; Chapman, K. W.; Chupas, P. J.; Yang, X. Q.; Grey, C. P. Origin of Additional Capacities in Metal Oxide Lithium-Ion Battery Electrodes. *Nat. Mater.* **2013**, *12*, 1130−1136.
(52) Manthiram, A.; Vadivel Murugan, A.; Sarkar, A.; Muraliganth, T. Nanostructured Electrode Materials for Electrochemical Energy Storage and Conversion. *Energy Environ. Sci.* **2008**, *1*, 621−638.
(53) Mukherjee, R.; Krishnan, R.; Lu, T.-M.; Koratkar, N. Nanostructured Electrodes for High-Power Lithium Ion Batteries. *Nano Energy* **2012**, *1*, 518−533.
(54) Baxter, J.; Bian, Z. X.; Chen, G.; Danielson, D.; Dresselhaus, M. S.; Fedorov, A. G.; Fisher, T. S.; Jones, C. W.; Maginn, E.; Kortshagen, U.; Manthiram, A.; Nozik, A.; Rolison, D. R.; Sands, T.; Shi, L.; Sholl, D.; Wu, Y. Y. Nanoscale Design to Enable the Revolution in Renewable Energy. *Energy Environ. Sci.* **2009**, *2*, 559−588.